Anchorage of corroded bars: eccentric pull-out tests and numerical analysis

Anchorage of corroded bars: eccentric pull-out tests and numerical analyses

K. Zandi Hanjari
CBI Swedish Cement and Concrete Research Institute, Borås, Sweden
Chalmers University of Technology, Gothenburg, Sweden

D. Coronelli
Politecnico di Milano, Italy

K. Lundgren & M. Plos
Chalmers University of Technology, Gothenburg, Sweden

ABSTRACT: Eccentric pull-out tests were carried out to study (a) the influence of cover cracking and (b) the effect of stirrups, on the bond of corroded bars. Next, an earlier developed corrosion model was extended to include the effect of rust flowing through corrosion cracks. The extended model was used in detailed three-dimensional analyses of the tests. The tests and analyses showed an important effect of the cover cracking in terms of loss of confinement and the flow of rust through the cracks. They also indicated that the bond behavior and the failure were strongly governed by the position of the anchored bar, i.e. corner or middle positions, and the level of the corrosion attack. Stirrups played an important role after cover cracking, as they then became the primary source of confinement. Furthermore, corrosion of stirrups led to a more extensive cover cracking for a relatively low level of corrosion attack.

1 INTRODUCTION

Many existing concrete structures, for example bridges, piers and parking garages, show significant corrosion; in the presence of high levels of corrosion it is not uncommon that cover cracking, spalling and delamination have occurred. The consequent reduction of bond strength can well be a major problem for the performance of structures in the service and ultimate states, see Val (2007), Vidal et al. (2007), Coronelli & Gambarova (2004) and Rodriguez et al. (1995). The study of concrete cracking due to corrosion during the service life is necessary to assess the durability of the structure over time. In particular, crack width can be an indicator of structural distress, see Vidal et al. (2004). In the ultimate limit state, the loss of bond of the main reinforcement in anchorage regions affects the shear strength and anchorage capacity of beams, see Regan & Kennedy Reid (2009), Rodriguez et al. (1995), and Regan & Kennedy Reid (2004).

The effect of corrosion attacks on bond strength has been studied by several researchers, see e.g. Almusallam et al. (1996) and Clark & Saifullah (1993). Previous research on the corrosion cracking and bond of corroded reinforcement has however been mainly concerned with the corrosion of the main reinforcement of specimens without transverse steel. Very few researchers have studied and compared the corrosion induced cracking of test specimens with and without stirrups, see Alonso et al. (1998). Moreover, to the knowledge of the authors, the effect of corroded stirrups on bond strength has not previously been tested with pull-out tests. The tests presented in this paper address the two issues: (a) the influence of cover cracking and (b) the effect of stirrups, on the bond of corroded bars.

Three-dimensional finite element modeling has proved to be capable of describing the behavior of reinforced concrete in a comprehensive way, provided that appropriate constitutive models are adapted. Furthermore, the effect of corrosion on the reinforcement, on the surrounding concrete and on their interaction can be simulated more realistically. Volume expansion of corrosion products, that leads to cover cracking and spalling, significantly influences the confinement conditions and consequently the steel/concrete bond. These effects have been taken into account in bond and corrosion models previously developed by Lundgren (2005a, 2005b). At large corrosion penetrations, the corrosion products penetrate into cracks and reach the external surface of the cover, Berra *et al.* (2003). Under such conditions, when wide cracks develop, the favorable effect of rust flowing through the cracks becomes significant. This may reduce the pressure around the corroded bars, and consequently may reduce the damage to the surrounding concrete. Slow corrosion rates provide sufficient time so that rust penetration may effectively take place. This has been seen in real structures exposed to natural corrosive environments. The previously developed corrosion model, Lundgren (2005b), was extended to include this phenomenon. The theoretical framework of the bond and corrosion

models, as well as the principles of further development of the corrosion model to account for the effect of rust flowing through a crack, are discussed in this paper. Furthermore, the eccentric pull-out tests were simulated using the extended corrosion model in detailed three-dimensional non-linear finite element analyses.

2 EXPERIMENTS

2.1 *Test set-up and program*

A research program comprising both the study of corrosion cracking and bond strength deterioration was undertaken. The aim was to better understand the effects of cover cracking and of corroding stirrups on bond behavior in anchorage regions. Details about the tests are given in a report, Zandi Hanjari & Coronelli (2010) and Zandi Hanjari et al (2011a). Some aspects of the experimental program and results are summarized here.

The eccentric pull-out specimens had the shape of a beam-end after inclined shear cracking, see Figure 1. The behavior of the eccentric pull-out tests shares some similarities and dissimilarities with a beam-end region. For example, similar to a beam-end region, the inclined strut is carried on both the anchored bar and the support region. However, in the test specimens, the main bars were not in contact with the concrete over the support. The effect of support pressure and the anchorage of the bar over the support are therefore not the same as they are at the end of a beam.

Test specimens were cast with a concrete of grade C30/37 mixed in two batches: Mix I with 3% sodium chloride and Mix II without sodium chloride, Table 1. The influences of the location of the anchored bar, i.e. middle or corner placement; the presence or absence of transverse reinforcement; the corrosion level of longitudinal reinforcement and the corrosion of transverse reinforcement were studied. The specimens were of three types in relation to the reinforcement arrangement and corrosion: specimens without stirrups, where the main bars were corroded (type A); specimens with stirrups where the main bars were corroded and the stirrups were protected by insulating tape (type B); and specimens with stirrups where the main bars and stirrups were corroded (type C), see Figure 1.

Table 1. Material properties.

Mix	$f_{cc,cube}$ [MPa]	$f_{cc,cylinder}$ [MPa]	f_{ct} [MPa]	G_F* [N/m]	E_c* [GPa]
I	37.5	29.7	2.3	64.3	29.4
II	34.5	27.7	2.2	61.2	28.7

* calculated based on Eurocode 2

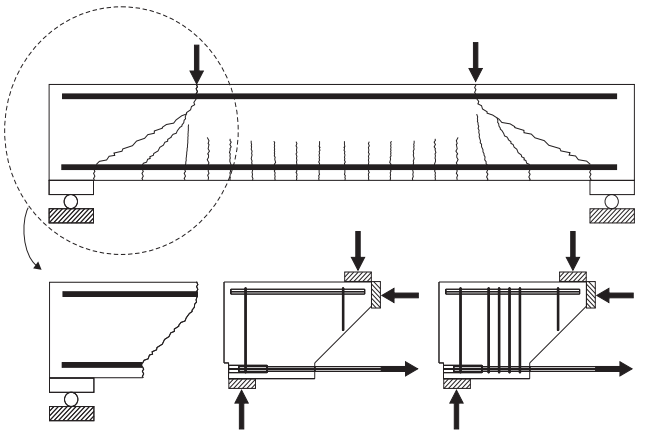

Figure 1. Schematic illustration of test set-up and specimens.

All of the specimens were subjected to accelerated corrosion, with an average current density of 100 μA/cm^2, for three time spans that caused a rebar weight loss up to approximately 20% in the main bars and 35% in the stirrups.

2.2 *Overview of test results*

All of the specimens showed longitudinal cracks along the main bars for relatively low corrosion levels. The corrosion level at first cracking was about 0.6% - 1.0% corrosion weight loss; the cracks widened with increased corrosion levels. Crack patterns formed depended on the presence or absence of stirrups and whether the stirrups were corroded.

An overview of the pull-out test results in comparison with the reduction in residual bond strength for corroded reinforcement, given by CEB-FIP Model Code 2010 is shown in Figure 2. The bond strengths of the eccentric pull-out specimens were normalized with respect to that of the reference specimens; this was done separately for the specimens with and without stirrups. In general, the average bond strength of specimens with stirrups was less influenced by corrosion than that of the specimens without stirrups. This shows the importance of the confinement provided by stirrups after cover cracking. The largest bond deterioration was seen in the type A specimens on the corner bars; this was because of the absence of stirrups and a smaller portion of surrounding concrete available to a corner bar compared with that of a middle bar. The least bond deterioration was measured in type B specimens on the corner bars. This is believed to be caused by the effective interaction between the stirrups and the main bars at the angle of the corner. It can be concluded that, for large corrosion penetrations that cause extensive cover cracking, stirrups play an important role in terms of being the main source of confinement. Moreover, the deterioration trend proposed by CEB-FIP Model Code 2010, when compared with the test results, remained on the safe side.

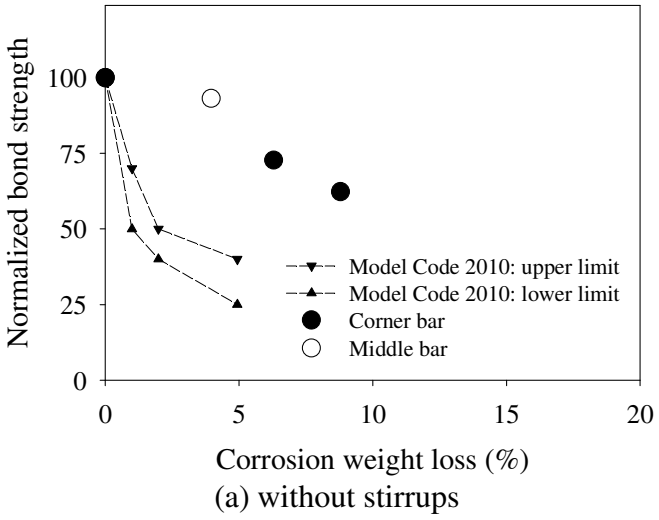

(a) without stirrups

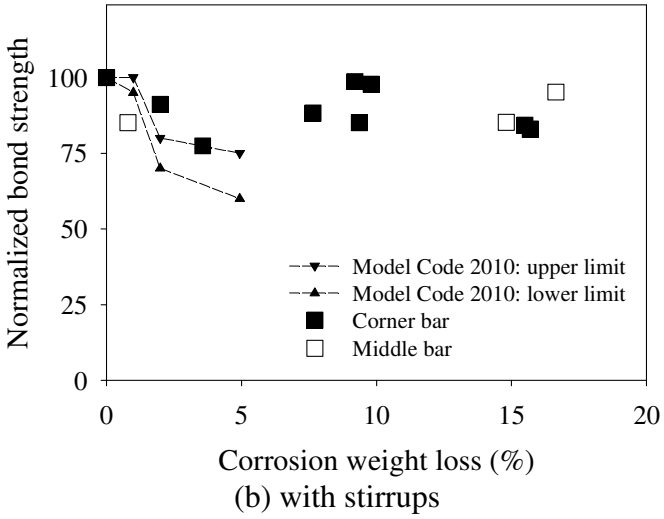

(b) with stirrups

Figure 2. Overview of the test results in terms of bond strength versus corrosion attack.

3 NUMERICAL ANALYSIS

3.1 *Original bond and corrosion models*

The bond model, first formulated in Lundgren & Gylltoft (2000) and later modified in Lundgren (2005a), has been calibrated for both monotonic and cyclic loading. The modeling approach is especially suited for detailed three-dimensional finite element analysis, where both the concrete and the reinforcement are modeled with solid elements. Surface interface elements are used at the steel/concrete interaction to describe a relation between the traction, σ, and the relative displacement, u, in the interface.

This bond model is a frictional one, using elasto-plastic theory to describe the relations between the stresses and the deformations. The relation between the tractions, σ, and the relative displacements, u, is in the elastic range:

$$\begin{bmatrix} \sigma_n \\ \sigma_t \\ \sigma_r \end{bmatrix} = \begin{bmatrix} D_{11} & 0 & 0 \\ 0 & D_{22} & 0 \\ 0 & 0 & D_{33} \end{bmatrix} \begin{bmatrix} u_n \\ u_t \\ u_r \end{bmatrix} \quad (1)$$

where D_{11} and D_{22} describe the relation between displacements and stresses in the radial and transverse directions, respectively. The third component, added for three-dimensional modeling, corresponds to the stress acting in the direction around the bar, i.e. D_{33} , is a dummy stiffness preventing the bar from rotation around its axis. This was assumed to be independent of the other components.

The yield lines of the model are described by two yield functions: one explains the friction, F_1, assuming that the adhesion is negligible, while the other, F_2, describes the upper limit at a pull-out failure, determined from the stress in the inclined compressive struts, which results from the bond action:

$$F_1 = |\sigma_t| + \mu\sigma_n = 0 \quad (2)$$

$$F_2 = \sigma_t^2 + \sigma_n^2 + c \cdot \sigma_n = 0 \quad (3)$$

More details concerning yield lines, flow rules, and hardening laws have been given in Lundgren (2005a). The model, used in simulation of several pull-out tests, gave results which were in good agreement with the experiments.

The corrosion model was developed in Lundgren (2002) and further calibrated with several tests in Lundgren (2005b). The effect of corrosion has been modeled as the volume increase of the corrosion products when compared with the virgin steel. The volume of the rust relative to the uncorroded steel, υ_{rs}, and the corrosion penetration, x, as a function of the time were used to calculate the free increase of the bar radius, r, i.e. the increase in radius including the corrosion products when the normal stresses were zero. Then the corrosion was modeled by taking time steps. The free increase of the radius was calculated from:

$$y = -r + \sqrt{r^2 + (\upsilon_{rs} - 1) \cdot (2rx - x^2)} \quad (4)$$

The real increase of the radius, u_{ncor}, is smaller due to the confinement from the surrounding concrete. This results in a total strain in the rust, ε_{cor}:

$$\varepsilon_{cor} = \frac{u_{ncor} - y}{x + y} \quad (5)$$

From the normal strain in the rust, corresponding stresses normal to the bars surface were determined. Few studies have been made to describe the mechanical behavior of rust, see Molina *et al.* (1993). Experimental results in corrosion cracking tests have been combined with finite element analyses; it has been concluded that rust behaves as a granular material, i.e. its stiffness increases with the stress level, see Lundgren (2005b). This was later verified to be a good estimation of rust behavior, see Ouglova *et al.* (2006). In the corrosion model, it was assumed that the mechanical behavior of the rust at loading could be described as

$$\sigma_n = K_{cor} \cdot \varepsilon_{cor}^{p} \quad (6)$$

where K_{cor} represents the stiffness of the corrosion products in the radial direction, ε_{cor} is the strain in the rust, and p is an exponent to describe the granular behavior.

The corrosion model and the bond model can be viewed as two separate layers around a reinforcement bar. However, they are integrated in one interface element to reduce the number of nodes required to model a structure. Due to equilibrium between the two layers, the traction, σ, is the same in the bond and in the corrosion layers. The deformations are related as:

$$u_n = u_{ncor} + u_{nbond} \quad (7)$$

$$u_t = u_{nbond},\ u_{tcor} = 0 \quad (8)$$

where the index *cor* means the corrosion layer, and the index *bond* means the bond layer. The equations (7) and (8) are solved within the interface element together with the condition for equilibrium using an iterative procedure.

3.2 *Further development of the corrosion model*

The eccentric pull-out tests, presented in Section 2, showed that when the first corrosion crack took place, corrosion products started to flow through cracks and reached the outer surface of the concrete. For large corrosion penetrations, when several new cracks initiated and widened, the flow of rust became significant. This decreased the splitting stress around the bar and consequently reduced the damage to the surrounding concrete. The flow of rust not only depended on the number of cracks and crack width but also varied in time. During the time in which the specimens were subjected to corrosion, the flow of corrosion products took place continuously.

In this work, a detailed study of the phenomenon involved in the flow of corrosion product through cracks was not a goal. The main concern was to draw attention to the observations made in laboratory tests and to show the consequence of this type of effect by using numerical analysis. Therefore, several simplified assumptions were made on physio-chemical properties of rust and the crack through which rust flows. For instance, the physical state of corrosion products may strongly depend on the oxide composition and the relative humidity in the crack. Moreover, the geometry of the crack in which rust flows may also influence the phenomenon. As there is a lack of such information in the literature, it was assumed that rust behaves as a plug material. More details concerning this phenomenon and the assumptions are clearly stated in Zandi Hanjari (2011b).

The previously developed corrosion model, Lundgren (2005b), was extended to include the rust flow effects. A summary of the further development of the model are presented here; details concerning assumptions and the derivation of equations together with the discussion of the model was presented in Zandi Hanjari (2011b). It was assumed that the volume flow of rust depends on the corrosion time interval, crack width and the normal stress in the rust layer. The corrosion time and corrosion rate were given as input to the model. Corrosion penetration, x, was determined theoretically based on Faraday's law according to:

$$x = 5.85 \cdot (t \cdot I) \quad (9)$$

where x is corrosion penetration in μm; t is corrosion time in year; and I is impressed current in μA/cm^2. The crack width, w_{cr}, was computed from the nodal displacements across the crack. The section area of the crack, through which rust flows, was calculated as:

$$A_{cr} = w_{cr}.e \quad (10)$$

where A_{cr} is the section area of the crack, w_{cr} is the crack width and e is the element size along the crack; see Figure 3. The splitting stress, as in the earlier version of the corrosion model, was evaluated from the strain in the rust using equation (6). The total volume flow of rust, V, through a crack is calculated as the summation of the volume flow of rust in time steps (increments), ΔV_i, as

$$V = \sum_{i=1}^{k} \Delta V_i \quad (11)$$

where index i is the time increment number. The volume flow of rust through a crack, within a time increment, Δt_i , was expressed by:

$$\Delta V_i = \left[v_{i-1} + \frac{1}{2}\left(\frac{A_{cr,i-1} \cdot \sigma_{n,i-1}}{\rho(V_{i-1} + \Delta V_i)} \cdot \Delta t_i \right) \right] \cdot A_{cr,i-1} \cdot \Delta t_i \quad (12)$$

where v is the velocity of the rust flow; σ_n is the splitting stress according to equation (6); and ρ is the density of rust. With respect to the volume flow of rust, the free increase of radius of the corroded bar was given from geometry by:

$$y_{ext} = -r + \sqrt{r^2 + (\upsilon_{rs} - 1)(2rx - x^2) - \frac{V}{\pi \cdot e}} \quad (13)$$

where y_{ext} is the free increase of the radius due to the remaining rust around the corroded bar, r is the original bar radius and υ_{rs} is the volume of the rust relative to the uncorroded steel. Thereafter, the strain in the rust, ε_{cor}, is calculated similar to that in the original model using equation (5). The deformation in the interface layer, divided between the bond layer and the corrosion layer, is computed by solving

equations (7) and (8) together with the condition for equilibrium using an iterative procedure.

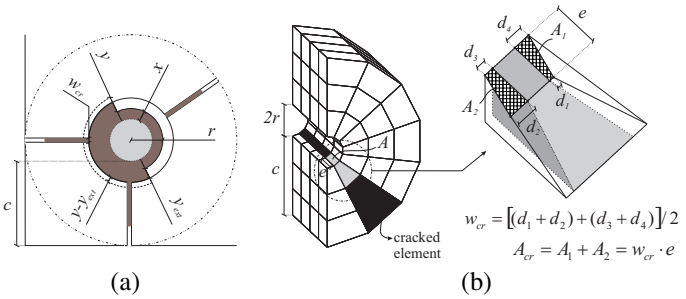

Figure 3. (a) Physical interpretations of the variables in the extended corrosion model; and (b) section area of the crack through which rust flows.

3.3 *Modeling of eccentric pull-out tests*

The eccentric pull-out tests were analyzed in detail using non-linear three-dimensional finite element (FE) models by use of the FE program DIANA. The analyses were carried out in two phases. In the first phase, the corrosion attack was applied in time steps as the expansion of the corrosion products. In the second phase, the external pull-out force was gradually imposed on the tested bar according to the prescribed displacement. An incremental static analysis was made using a Newton-Raphson iterative scheme to solve the non-linear equilibrium equations.

Due to symmetry, half of the specimen was modeled with an approximate element size of 10 mm, Figure 4. Four-node, three-sided isoparametric solid pyramid shaped elements were used for the concrete, transverse and longitudinal reinforcements. For concrete, a constitutive model based on non-linear fracture mechanics using a smeared rotating crack model based on total strain was applied. The crack band width was assumed to be equal to the element size; this was later verified to be a good approximation of the localization zone in the analyses. For the concrete in compression and tension, the models by Thorenfeldt et al. (1987) and Hordijk (1991), respectively, were adopted. The reinforcing steel was modeled according to an isotropic plastic model with the Von Mises yield criterion. The material properties for the concrete were the same as given in Table 1.

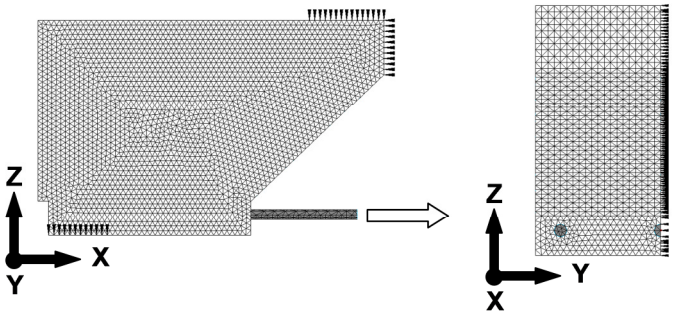

Figure 4. Finite element mesh with the boundary conditions.

As in the experiments, the longitudinal bars were subjected to corrosion attack from one direction, i.e. half of the main bar cross section was affected by corrosion. The corrosion attack imposed on half of the main bar cross section was equivalent to the total bar weight loss measured along the embedment length. The bottom leg of the stirrups was subjected to corrosion all around the cross section. The vertical leg of the stirrups was corroded halfway up to the longitudinal bar section. These choices corresponded to the experimental observations. In the experiment, the corrosion penetration depth differed between different bars. In the analyses with the original corrosion model, however, the same corrosion penetration depth was imposed on all of the main bars; this corrosion attack corresponds to the corrosion penetration depth of the bars tested shortly before the pull-out test. In the analyses with the extended corrosion model, the same corrosion attacks as in the experiments were imposed on each bar.

4 RESULT AND DISCUSSION

4.1 *Corrosion phase*

Corrosion-induced crack patterns in terms of the maximum tensile strains from the numerical analyses with extended corrosion model are shown in Figure 5. The analysis with the original model could only be carried out to a corrosion attack equivalent to rebar weight losses of 1.4%, 1.7% and 0.3% for specimen types A, B and C, respectively. This corrosion attacks corresponded to extensive cover cracking; for higher corrosion attacks, severe damage of concrete resulted in numerical instability in the analysis. The difference in the corrosion attacks that caused extensive cover cracking and termination of the analyses for the three types of specimens was related to the amount of confinement, i.e. the presence

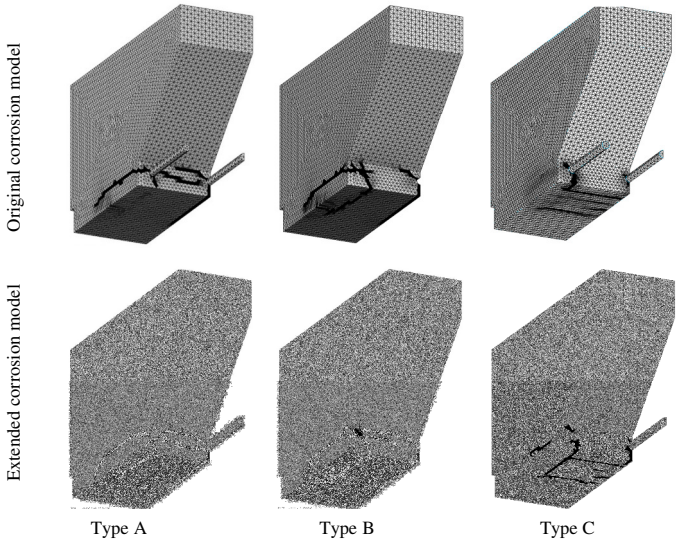

Figure 5. Corrosion-induced crack patterns in terms of the maximum tensile strains from numerical analyses.

or absence of stirrups and whether or not the stirrups were corroded. However, the analyses with the extended model could be continued with larger corrosion penetration depths. This is an important advantage when the extended corrosion model is used.

Three main cover cracking patterns were observed in the numerical analysis. In the absence of stirrups, specimen type A, the corrosion-induced cracks around the corner bars propagated in a direction with the least resistance. For this reason, a corner cover spalling took place. In specimen type B, the corrosion-induced cracks, initiated from the corner and middle bars, propagated across the cross-section and formed a delamination plane. A different pattern was obtained when both longitudinal and transverse bars were corroded, specimens type C. In this situation, wide cracks appeared transversely to the main bars, due to corroding stirrups, before any of the former patterns occurred. Thus a more local cover crack pattern, mainly damage of the concrete between the stirrups, formed. As the concrete cover was smaller over the stirrups, the splitting cracks appeared for a relatively low corrosion attack. All the three types of crack patterns agreed well with the experimental observation.

4.2 *Pull-out phase*

The results from numerical analysis with the extended corrosion model, in terms of the maximum tensile strains representing crack pattern and average bond stress versus free-end slip, are presented in Figures 6 and 8, respectively. The behavior of the specimens without stirrups, type A, was relatively well predicted, both in the corner bar test and the middle bar test. The agreement was less good when the specimens had stirrups and especially when the stirrups were corroded. Generally, less bond capacity for the corroded bars was obtained in the analysis than that measured in the experiments.

A typical crack pattern and crack widths from the experiment for type C specimen are shown in Figure 7. The load measured on each bar was divided by the surface area of the bar along the embedment length to calculate the average bond stress. The results are plotted for the analyses with the extended corrosion model and the experiments in Figure 8. The numerical analyses showed good correspondence with the tests results, confirming the failure modes and crack pattern obtained in the tests. The analyses also gave reasonably good results in terms of bond stress versus slip. One small difference between tests and analyses concerns the slip for the uncorroded specimens; the analyses result in weaker behavior with slightly larger slip values for the ascending branch than the test results. This behavior can also be seen in earlier analyses with the bond model used, see e.g. Lundgren, (2005a and 2005b). The main reason for this difference is that the main focus when the bond model was calibrated was the ultimate limit state, with anchorage failure. Thus the bond model needs to be better calibrated for small slip values.

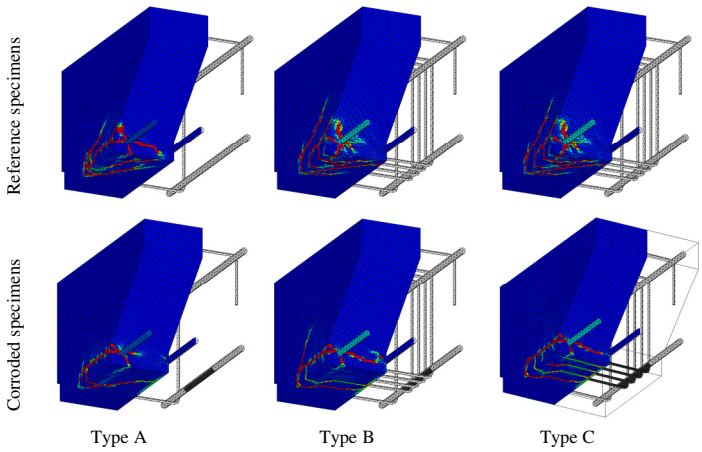

Figure 6. Crack patterns, in terms of the maximum tensile strains, of specimens subjected to pull-out.

The behavior of the specimens without stirrups, type A, was well predicted, both in the corner bar test and the middle bar test. The agreement was less good when the specimens had stirrups and especially when the stirrups were corroded; the analyses underestimated the capacity. The experimental results showed very little difference between specimen types B and C for similar corrosion attacks, while the analysis results indicated a larger effect of corroded stirrups. The experimental observations showed that the concrete cover in both type A and B specimens were extensively cracked due to corrosion, although the crack patterns differed. Type C specimens had cracks that were more distributed and also had several transverse cracks at the position of the stirrups, with a smaller crack width than that in type A specimens, see Figure 7. The crack pattern obtained in the analyses of type C specimens only showed the large cracks seen in the experiments; the cracks with a small opening did not occur in the analysis. Furthermore, the crack widths obtained in the analyses of type C specimens were much larger than that measured in the experiments. This might explain the underestimation of the bond capacity in the numerical analysis, as large cracks significantly reduce the confinement and consequently lead to a larger bond deterioration.

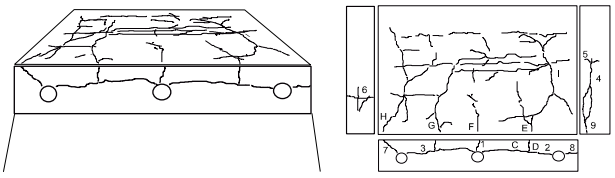

Crack no.	1	2	3	4	5	6	7	8	9	C	D	E	F	G	H	I
Width (mm)	0.3	0.3	0.3	0.35	0.2	0.15	0.3	0.45	0.35	0.45	0.2	0.25	0.2	0.15	0.2	0.3

Figure 7. Crack pattern and crack widths from the experiments for a type C specimen.

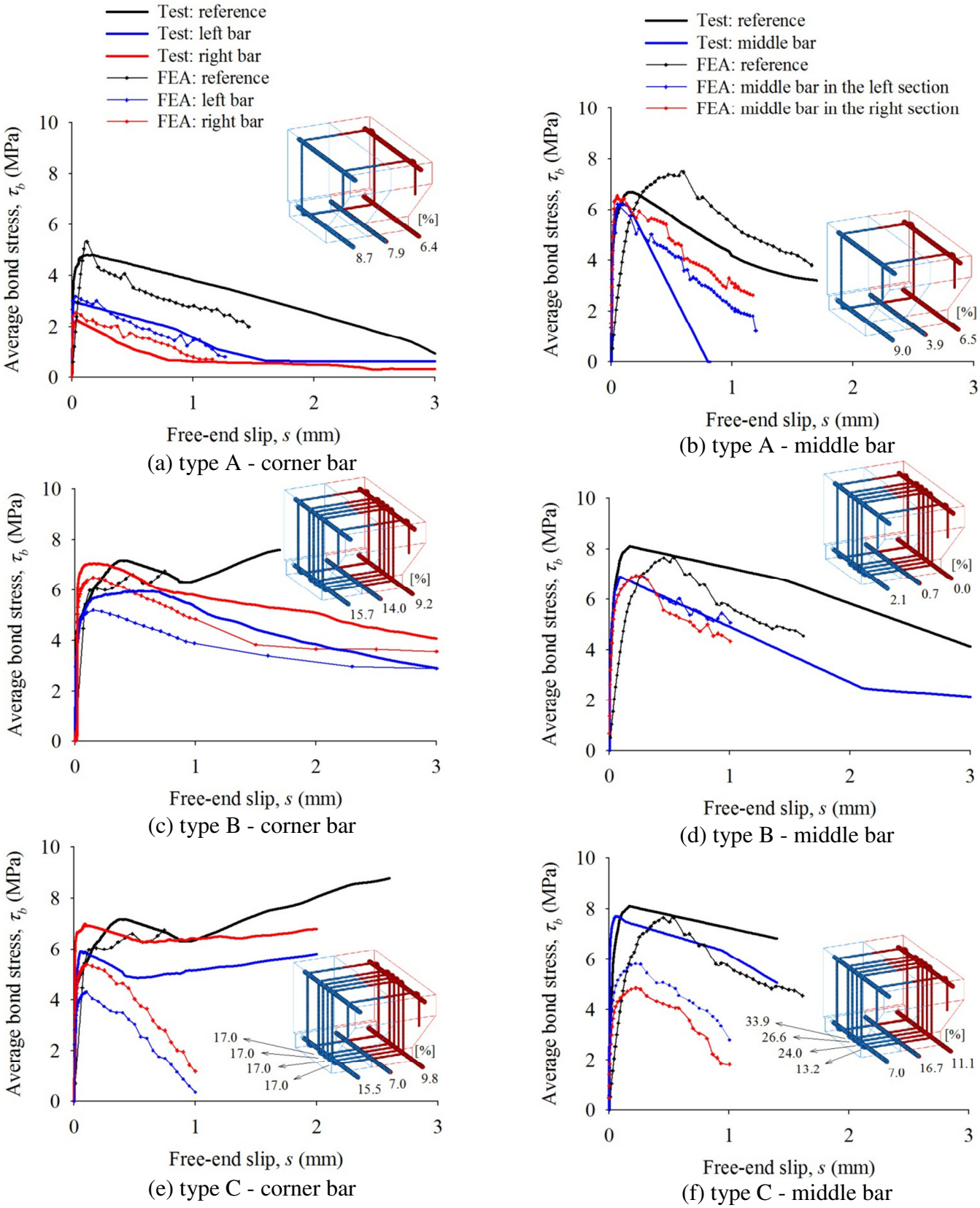

Figure 8. Average bond stress versus free-end slip from numerical analyses and experiments

5 CONCLUSIONS

The effect of extensive corrosion of main bars and stirrups on the behavior of anchored bars at corner and middle positions was investigated. When high corrosion attacks occur in reinforced concrete structures and wide cracks develop, the effect of corrosion products flowing through cracks becomes significant and leads to a decrease in the splitting stress around the bar. The structure is therefore subjected to less damage. A previously developed corrosion model was extended to include this phenomenon. The extended corrosion models were used in analyses of eccentric pull-out tests and the results, in terms of corrosion-induced crack pattern and bond capacity, were compared with those measured in the experiments. The following conclusions are drawn on the basis of this study.

(1) The test results showed the significant influence of the stirrups, the position of the tested bar and the corrosion on the bond capacity and the failure mode.

(2) When the main bars were corroded, the highest anchorage capacity was measured for a middle bar in the presence of uncorroded stirrups, while the lowest capacity was measured for a corner bar in the absence of stirrups.

(3) The extended corrosion model used in the analyses of eccentric pull-out tests gave results that were consistent with what was observed in the experiments. The results indicated the important effect of the phenomenon on corrosion-induced damage, crack width and bond strength.

(4) Due to the favorable effect of corrosion products flowing through cracks, less damage was observed in the analyses with the extended corrosion model; this corresponds well with the experimental observations. Numerical instability due to extensive cracking of concrete was thus delayed in the analyses that used the extended corrosion model.

(5) In the extended corrosion model, the volume flow of corrosion products also depended on the corrosion rate. A high corrosion rate significantly reduces the corrosion time; a smaller volume of corrosion products thus flows through the crack. Greater differences in the results of the original and the extended corrosion models were seen when a low corrosion rate was adopted.

(6) Several assumptions were made to simplify the formulation of the extended corrosion model. For example, the friction in the crack (for the flow of corrosion products) and the change of the crack width along its depth were not taken into account. Moreover, owing to a lack of information concerning the physical state of the corrosion products, the density of corrosion products was assumed to be constant. These assumptions must be studied further.

6 REFERENCES

Almusallam, A. A., AlGahtani, A. S., Aziz, A. R., Dakhil, F. H. and Rasheeduzzafar. 1996. Effect of reinforcement corrosion on flexural behavior of concrete slabs. *Journal of Materials in Civil Engineering,* Vol. 8, No 3, pp. 123–127.

Alonso, C., Andrade, C., Rodriguez, J. and Diez, J. M. 1998. Factors controlling cracking of concrete affected by reinforcement corrosion. *Materials and Structures/Materiaux et Constructions.* Vol. 31, No. 211, pp. 435–441.

Berra, M., Castellani, A., Coronelli, D., Zanni, S. and Zhang, G. 2003. Steel-concrete bond deterioration due to corrosion: Finite-element analysis for different confinement levels. *Magazine of Concrete Research,* Vol. 55, No. 3, pp. 237–247.

CEB 2010. *CEB-FIP Model Code 2010 - First complete draft.* Bulletin 55, Volume 1, Lausanne, Switzerland.

Clark, L. A. and Saifullah, M. 1993. Effect of corrosion on reinforcement bond strength. *Proceeding of the 5th International Conference on Structural Faults and Repairs*, Edinburgh, pp. 113–119.

Coronelli, D. and Gambarova, P. 2004. Structural assessment of corroded reinforced concrete beams: Modeling guidelines. *Journal of Structural Engineering,* Vol. 130, No. 8, pp. 1214–1224.

Hordijk, D. A. 1991. *Local Approach to Fatigue of Concrete.* Doctoral thesis, Delft University of Technology, Delft, Netherlands.

Lundgren, K. and Gylltoft, K. 2000. A model for the bond between concrete and reinforcement. *Magazine of Concrete Research,* Vol. 52, No. 1, pp. 53–63.

Lundgren, K. 2002. Modelling the effect of corrosion on bond in reinforced concrete. *Magazine of Concrete Research,* Vol. 54, No. 3, pp. 165–173.

Lundgren, K. 2005a. Bond between ribbed bars and concrete. Part 1: Modified model. *Magazine of Concrete Research,* Vol. 57, No. 7, pp. 371–382.

Lundgren, K. 2005b. Bond between ribbed bars and concrete. Part 2: The effect of corrosion. *Magazine of Concrete Research,* Vol. 57, No. 7, pp. 383–395.

Molina, F. J., Alonso, C. and Andrade, C. (1993). Cover cracking as a function of rebar corrosion. 2. Numerical model. *Materials and Structures,* Vol. 26, No. 163, pp. 532–548.

Ouglova, A., Berthaud, Y., François, M. and Foct, F. 2006. Mechanical properties of an iron oxide formed by corrosion in reinforced concrete structures. *Corrosion Science,* Vol. 48, No. 12, pp. 3988–4000.

Regan, P. E. and Reid, I. L. K. 2004. Shear strength of RC beams with defective stirrup anchorages. *Magazine of Concrete Research,* Vol. 56, No. 3, pp. 159–166.

Regan, P. E. and Kennedy-Reid, I. 2009. Assessment of concrete structures affected by delamination: 1 - Effect of bond loss. *Studies and Research - Annual Review of Structural Concrete,* Vol. 29, pp. 245–275.

Rodriguez, J., Ortega, L. M. and Casal, J. 1995. *The Residual Service Life of Reinforced Concrete Structures: Relation between corrosion and load bearing capacity of concrete beams*. Report BRITE/EURAM PROJECT BREU CT92 0591.

Thorenfeldt, E., Tomaszewicz, A. and Jensen, J. J. (1987). Mechanical properties of high-strength concrete and applications in design. *Conference on Utilization of High-Strength Concrete.* Stavanger, Norway.

Val, D. V. 2007. Deterioration of strength of RC beams due to corrosion and its influence on beam reliability. *Journal of Structural Engineering,* Vol. 133, No. 9, pp. 1297–1306.

Vidal, T., Castel, A. and François, R. 2004. Analyzing crack width to predict corrosion in reinforced concrete. *Cement and Concrete Research,* Vol. 34, No. 1, pp. 165–174.

Vidal, T., Castel, A. and François, R. 2007. Corrosion process and structural performance of a 17 year old reinforced concrete beam stored in chloride environment. *Cement and Concrete Research,* Vol. 37, No. 11, pp. 1551–1561.

Zandi Hanjari, K. and Coronelli, D. 2010. Anchorage Capacity of Corroded Reinforcement: Pull-out Tests on Beam-end Specimens. Report No. 2010-06, Department of Civil and Environmental Engineering, Chalmers University of Technology, Göteborg, Sweden, Dipartimento di Ingegneria Strutturale, Politecnico di Milano, Milan, Italy.

Zandi Hanjari, K., Coronelli, D. and Lundgren, K. 2011a. Bond capacity of severely corroded bars with corroded stirrups, *Magazine of Concrete Research,* 63(12), 953-968.

Zandi Hanjari, K., Lundgren, k., Plos, M. and Coronelli, D. 2011b. Three-dimensional modelling of structural effects of corroding steel reinforcement in concrete, Structure and Infrastructure Engineering.